Available online at www.sciencedirect.com
ScienceDirect
Progress in Natural Science 18 (2008) 851–860
Progress in Natural Science
www.elsevier.com/locate/pnsc

Structures, kinematics, thermochronology and tectonic evolution of the Ramba gneiss dome in the northern Himalaya

Lei Guo, Jinjiang Zhang *, Bo Zhang

The Key Laboratory of Orogenic Belts and Crustal Evolution, Ministry of Education, China
School of Earth and Space Sciences, Peking University, Beijing 100871, China

Received 1 November 2007; received in revised form 8 January 2008; accepted 8 January 2008

Abstract

The Ramba gneiss dome, one of the north Himalayan gneiss domes, is composed of three tectono-lithologic units separated by an upper and a lower detachment fault. Low-grade metamorphic Tethyan Himalayan sedimentary sequence formed the upper unit above the brittle upper detachment fault. Mylonitic gneiss and a leucogranite pluton made up the lower unit beneath the ductile lower detachment fault. Mylonitic middle-grade garnet-, staurolite- and andalusite-schist constituted the middle unit between the two faults, which may be that the basal part of the upper unit experienced detachment shear. The Ramba dome underwent three episodes of deformation in its tectonic evolution. The first episode was a top-down-to-north-northwest sliding possibly related to the activity of the south Tibetan detachment system (STDS). The second episode was the dominant deformation related to a east–west extension, which resulted in a unique top-down-to-east kinematics and the major tectonic features of the dome. The third episode was a collapse sliding toward the outsides of the dome. The Ramba gneiss dome is possibly a result of the east–west extension and magmatic diapir. The lower detachment fault is probably the main detachment fault separating the sedimentary sequence from the crystalline basement during the east–west extension in the dominant deformation episode. The diapir of the leucogranite pluton formed the doming shape of the Ramba gneiss dome. This pluton intruded in the core of the dome in a late stage of the dominant deformation, and its Ar–Ar cooling ages are about 6 Myr. This indicates that the dominant deformation of the dome happened at the same time of the east–west extension represented by the north–south trending rifts throughout the northern Himalaya and southern Tibet. Therefore, the formation of the Ramba gneiss dome should be related to this east–west extension.

Keywords: Ramba gneiss dome; North Himalayan gneiss domes; East–west extension

1. Introduction

The north Himalayan gneiss domes (NHGD) [1–7], south Tibetan detachment system (STDS) [8–11] and north–south trending rifts [12–21] are important representatives of the extensional structures formed in Tibetan Plateau since Miocene [22]. Gneiss domes developed widely in the NHGD. Most domes are cored by muscovite-biotite granite or leucogranite plutons, mantled by deformed gneisses and overlain by lower-grade metamorphosed Paleozoic-Cenozoic Tethyan Himalayan sedimentary sequence. Medium-grade metamorphic equivalents of this sedimentary sequence, e.g. phyllite and garnet schists, were possibly interlayered between the gneisses and lower-grade rocks. These domes have exposed granites and rocks in depth, which afforded a window to research the tectonic evolution of the northern Himalaya, and therefore the domes have become a study focus in Himalayan geology [1–7,23–27].

At present, many different formation mechanisms have been put forward for the north Himalayan gneiss domes.

* Corresponding author. Tel.: +86 10 62754368; fax: +86 10 62751159.
E-mail address: zhjj@pku.edu.cn (J. Zhang).

1002-0071/$ - see front matter © 2008 National Natural Science Foundation of China and Chinese Academy of Sciences. Published by Elsevier Limited and Science in China Press. All rights reserved.
doi:10.1016/j.pnsc.2008.01.016

These models can be roughly classified into three catalogues: flow deformation in depth, crustal shortening and crustal extension. Flow deformation in depth includes diapirism, mantle upwelling and channel flow. In the diapiric model, the domes were thought to be formed by the buoyantly rising magmas coming from the anatexis above the MCT [28] or from depressed remelting caused by extension [9,23,29,30]. In mantle upwelling, the domes were thought to be formed by upwelling of asthenosphere due to lateral compression [16]. Channel flow model thought the ductile flow was caused by the melting layer of lower crust [31,32]. Crustal shortening model supposed the domes to be fault-bend folds developed above either a simple thrust ramp or a thrust duplex system [1,3,4,33,34]. Lee et al. suggested the domes were formed in a tectonic process in which contraction and extension happened simultaneously [6].

Kangmar, Mabja, Yalashangbo, Kampa, Malashan, Leo Pargil and Gurla Mandhata are some large domes in the NHGD (see Fig. 1 for the locations), and many comprehensive studies on them have been reported recently. Burg et al. [1] supposed the Kangmar dome to be a fault-bend fold formed above a thrust ramp or a thrust duplex. However, Chen et al. [2] argued that this dome was formed by a process similar to the formation of metamorphic core complexes in western USA, and it is an extensional feature in response to the gravitational collapse of the Himalayan topographic front. Based on detailed studies on Kangmar and Mabja domes, Lee et al. [5–7] proposed that the middle crustal extension followed by south-directed thrusting led to the high strain penetrative fabrics and domal geometry, the extension was related to the activities of the STDS. Zhang et al. [24] suggested that the lower detachment of Yalashangbo dome may be the exposure of the STDS in northern Himalaya. Tectonic denudation, exhumation and diapir of leucogranite formed the domal shape of the Yalashangbo dome [23,25]. Thiede et al. [26] reported the structure and chronology of the western part of Leo Pargil dome, suggesting the east–west extension since 16–14 Myr was the dominant cause for the formation of it. Murphy et al. [27] also concluded that the shearing of north–south trending Gurla Mandhata detachment faults since late Miocene exposed high-grade metamorphic rocks in depth and formed the Gurla Mandhata dome.

As a typical doming structure in the NHGD, Ramba gneiss dome was reported here with detail studies on its structural pattern and components, kinematics, thermochronology, and a discussion on the formation mechanism of this dome.

2. Regional setting

The NHGD is composed of a series of isolated gneiss domes exposed in the Tethyan Himalaya [8–11,35]. Overlying this region is a Cambrian-Eocene marine sedimentary sequence, the Tethyan Himalayan sedimentary sequence, deposited on the passive northern margin of the Indian continent [35,36]. The Tethyan Himalaya is structurally complex, exhibiting Cretaceous to Quaternary thrusts and folds [9,16,37–41] and extensional structures (e.g., the STDS and north–south trending rifts) [22]. The latest structures of this region are the north–south trending extensional structures since later Miocene to recent [12–21], such as the Yadong-Gulu rift and Xainza-Dinggye rift [18,20].

The Ramba gneiss dome reported here is one of the small doming structures located in the northern NHGD (Fig. 1). It has a surface shape like a heart and occupies

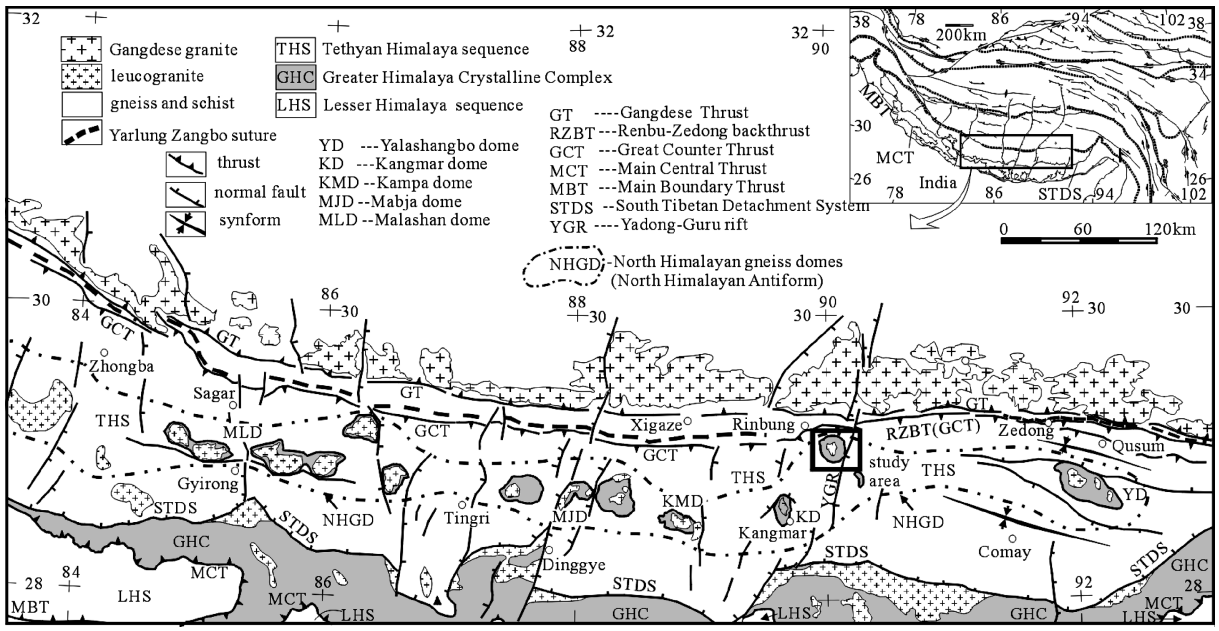

Fig. 1. Regional geological map of northern Himalaya, showing the north Himalayan gneiss domes and the study area (marked by a pane) in this paper (after Refs. [5,22,42]).

an area of about 400 km^2. Its exact geographic location is at 89°55′E–90°15′E and 29°00′N–29°12′N. The tectonic location of this dome belongs to the north–south trending Yadong-Gulu rift.

3. Tectono-lithologic units in the Ramba gneiss dome

The Ramba gneiss dome is cored by a leucogranite pluton which shows penetrative fabrics on its margin such as foliation and lineation. Two wrapped circular detachment faults developed around the dome, and we refer the outer one as the upper detachment fault and the inner one as the lower detachment fault, respectively. The two faults separated the metamorphic rocks beside the pluton into three lithologic units. From outer to inner of the dome or structurally from top to bottom, these units are successively the upper unit (low-grade metamorphic Tethyan sedimentary sequence), the middle unit (medium-grade garnet schists and phyllites) and the lower unit (mylonitic gneiss). The gneiss is intruded by leucogranite. The eastern flank of Ramba dome is truncated by a north–south trending normal fault (Fig. 2).

3.1. The upper unit: low-grade metamorphic Tethyan Himalayan sedimentary sequence

The low-grade metamorphic Tethyan Himalayan sedimentary sequence made up the upper unit. This sequence is composed of a series of marine sediments of late Triassic age. These rocks experienced low-grade metamorphism and most of them were metamorphosed to slate and phyllite. Their protolith was quartzite, sandstone and mudstone. The slaty cleavage of this unit basically dips outwards according to the dome shape. For example, it dips roughly northwards with dip angles of 20–40° on the northern flank of the dome, while it dips 50–60° in a northwest-western direction on the northwestern flank, and it dips 55° in a northeastern direction on the eastern flank (Fig. 2). The contact between this unit and the underlying middle unit is the upper detachment fault.

3.2. The upper detachment fault

The upper detachment fault developed in a circular shape around Ramba gneiss dome. It separated the slate and phyllite of the upper unit from the garnet schist of the middle unit (Fig. 2). On the western flank, slaty cleavage in the hanging wall dips 60° in a N20°E direction, whereas the schistose foliation in the footwall dips 55° westwards. The fault plane parallels the footwall foliation. On the northeastern flank, the fault plane dips 20° in a north-northeastern direction. Gabbro sills intruded along the fault and these rocks are chiefly composed of macrograins of pyroxene. The margins of these sills experienced strong deformation.

On the eastern flank of the Ramba gneiss dome, the upper detachment fault was truncated by a north–south trending normal fault (Fig. 3a). Cataclastic breccias developed in the fault zone, and down-dip striations can be seen on the fault plane. Steps on the fault plane indicated a down-dip sliding toward the east. Granite and gabbro sills (with large pyroxene grains) intruded along the fault and their margins experienced strong deformation. Marble can also be found in the fault belt which may be produced by thermal metamorphism. This normal fault has a north–south trending and it dips eastwards with a dip angle of 60°. According to the tectonic location, this fault should be one of the north–south trending normal faults in the Yadong-Gulu rift (Fig. 1, see Ref. [43]).

3.3. The middle unit: garnet-, staurolite- and andalusite-mica schist

This unit was confined by the upper detachment fault on the top and lower detachment fault on the bottom, respectively (Fig. 2). The metamorphic grade increases from top to bottom in this unit, and the rocks are accordingly composed of ilmenite-staurolite schist, garnet-staurolite two-mica schist, andalusite-garnet two-mica schist in the same sequence. The primary structures in the rocks have been transposed by penetrative deformation (Fig. 3e), but some domains preserve residual mineral assemblage and primary sedimentary bedding which indicate that the rocks were metamorphosed from sandstone, siltstone and mudstone. This rock association is similar to the overlying upper unit which belongs to the Tethyan Himalayan sedimentary sequence. The main mineral assemblage in this unit is quartz + feldspar + biotite + muscovite. Characteristic metamorphic minerals include garnet, staurolite, andalusite, tourmaline and ilmenite. Garnet grains have good crystal forms with zonal structure in them. Typical characters of mylonite occurred in the lower part of this unit due to strong deformation.

A few diabase and gabbro sills intruded along the foliation in the middle unit and they experienced the same deformation as their country rocks. Granitic mylonite was observed to occur along the foliation of the garnet schist on the northeastern side of the dome, and it may be formed by ductile deformation on a granite sill. The schist next to the lower detachment fault was intruded by many leucogranite and gabbro sills.

3.4. The lower detachment fault

This detachment fault placed the mylonitic schist of the middle unit over the mylonitic gneiss of the lower unit (Fig. 2). Shattered quartz vein mixed with cataclastic garnet schist and gneiss occurred in the fault zone on the northeastern side of the Ramba gneiss dome (Fig. 3b), where the fault plane dips 15° in a north-northeastern direction. On the northwestern side, asymmetric folds and tectonic lenses developed near the fault. Gabbro sills intruded along the fault and deformation strength in the sills increases from their centers to margins. The central

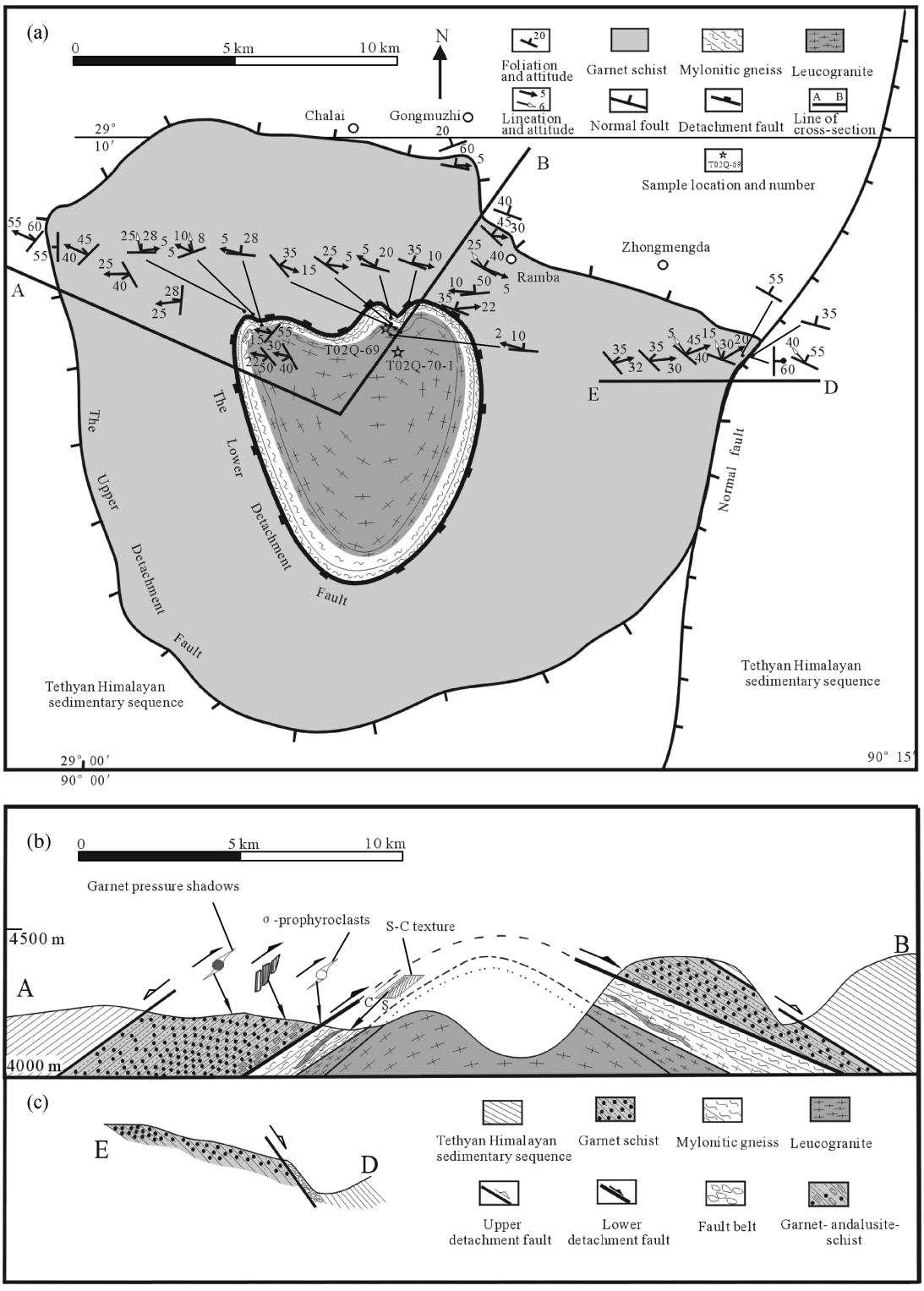

Fig. 2. Structural map of the Ramba gneiss dome (a), and the cross-sections (b and c).

part in a sill presents flow structure of macrograin; the parts next to the margins show preferred orientation of fine grains; the margins exhibit strong deformation with stretching lineation defined by extensively stretched pyroxene and feldspar grains, and foliation parallel to the fault plane. The zonation of deformation indicates that the gabbro sills intruded at the same time of the deformation.

3.5. The lower unit: mylonitic gneiss

Together with the core granite pluton, this unit made up the core of the Ramba gneiss dome beneath the lower detachment fault. This unit mainly consists of amphibolite and paragneiss which experienced strong deformation and were deformed into mylonitic rocks. The mylonitic folia-

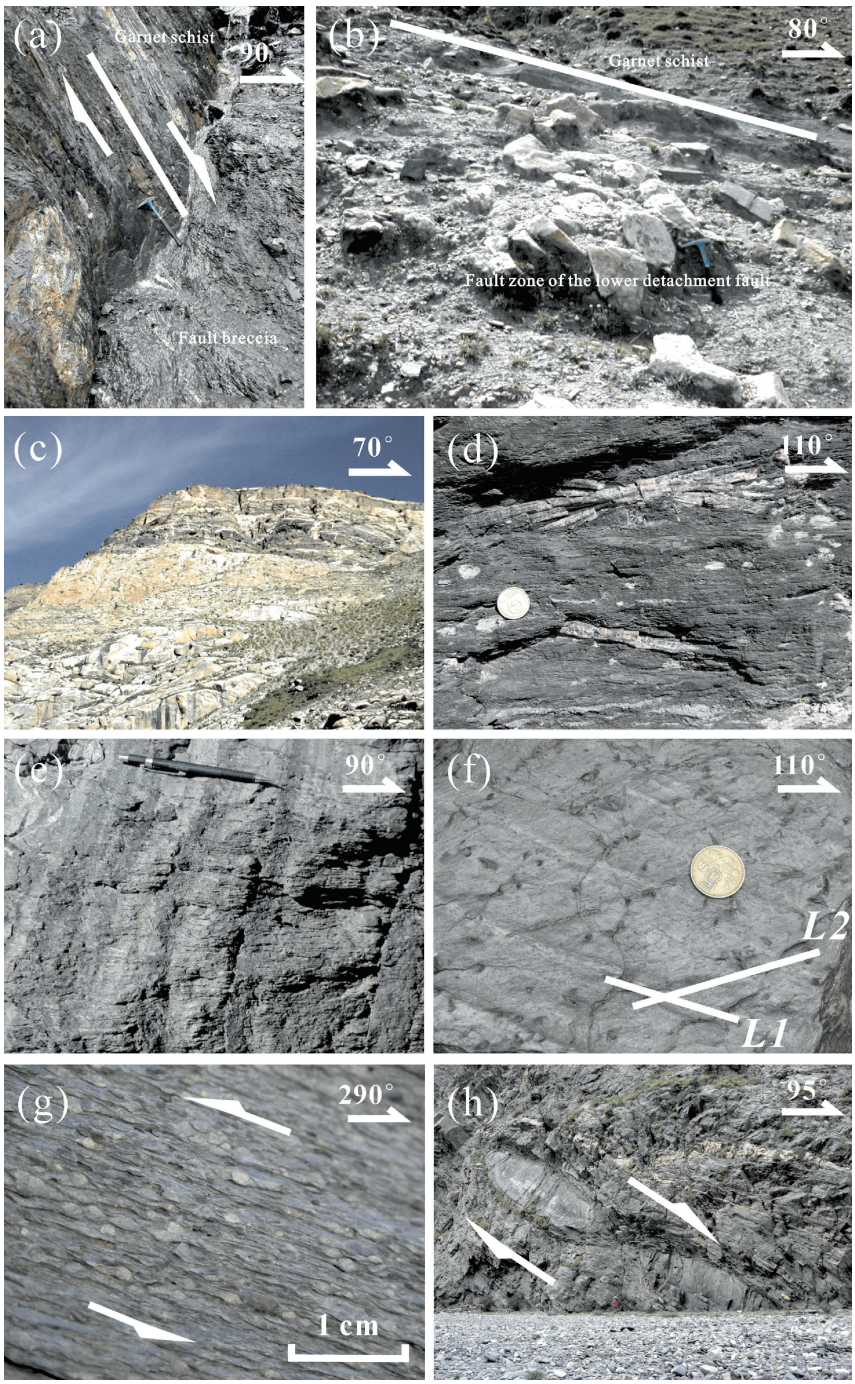

Fig. 3. Typical features and structures in the tectono-lithologic units of the Ramba gneiss dome. (a) The north–south trending normal fault on the eastern flank of the Ramba gneiss dome, the fault plane dip eastwards; (b) fault zone of the lower detachment fault; (c) contact between the granite pluton in the core and the overlying gneiss, the upper is the gneiss and the lower is the leucogranite; (d) garnet-andalusite-schist at the base of the middle unit, andalusite crystals cut the foliation but have a preferred orientation, indicating a thermal metamorphism in a later stage of the deformation; (e) foliation replacement in the middle unit; (f) two groups of lineation in the middle unit on the northwestern flank, L1 is the early north-northwest plunging lineation, L2 is the dominant west plunging lineation; (g) asymmetric structures in the middle unit on the northwestern flank, indicating a top-down-to-east shear; (h) large asymmetric puddings in the middle unit on the eastern flank, indicating a top-down-to-east shear.

tion is parallel to the lower detachment fault. The gneiss was intruded by leucogranite pluton in the core (Fig. 3c). The paragneiss is garnet-andalusite two-mica gneiss with a mineral assemblage of biotite + muscovite + quartz + plagioclase + garnet + andalusite. Enrichments of mica and quartz ribbons formed a banded structure. The mineral assemblage in the amphibolite is plagioclase + hornblende + biotite. On the northwestern side, pegmatite intruded along the foliation in the gneiss. Mineral assemblage of quartz + feldspar + muscovite + garnet indicates that the pegmatite belongs to leucogranite. The pegmatite experienced weak deformation.

3.6. Granite pluton of the core

The core of the Ramba gneiss dome is occupied by a granite pluton (Fig. 2). It has a mineral assemblage of quartz + plagioclase + orthoclase + muscovite + biotite (few) with enrichment in garnet and tourmaline. A garnet two-mica granite rim developed along the margin of the pluton, in which the content of plagioclase is a little more than the inner pluton. These two kinds of granite have a transitional relationship and intruded in a same magmatic event. Penetrative foliation and lineation were formed by alignment of mica grains, stretched quartz and feldspar in the margin of the pluton. The fabrics in the pluton have the same occurrence as their country rocks, but their intensity becomes weaker toward the core of pluton, and only weak alignment of minerals can be observed in the central part of the pluton. Remarkable thermal metamorphism can be seen in the country rocks next to the contact, which generated many andalusites with a length of about 10–15 cm (Fig. 3d). Andalusite crystals cut the foliation but have a preferred orientation, indicating that the core pluton may intrude in a later stage of the deformation.

4. Structures and kinematics

4.1. Lineation

Three groups of lineation were formed in the tectono-lithologic units of the Ramba gneiss dome (Fig. 4). The first group is the remnant stretching lineation with a nearly north–south plunging. The second group is the dominant and penetrative lineation which has a consistent east–west plunging. The third group is striations plunging outward the outside of the dome.

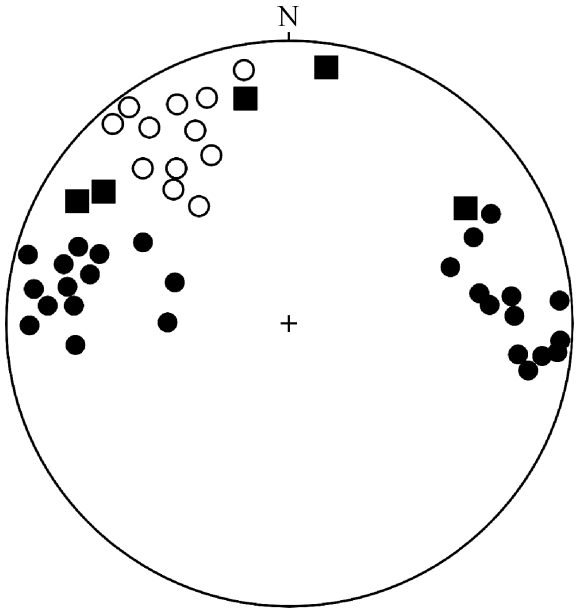

Fig. 4. Lower-hemisphere projections of the lineation in the Ramba dome on a Wulff net. Circles represent the early lineation; dots stand for the dominant lineation; black squares are the late striations.

The first group of lineation with a north–south plunging can be observed in the upper and middle units of the Ramba gneiss dome. It is defined by the alignment of metamorphic minerals and stretched quart. The lineation has a consistent nearly north–south plunging. It plunges to a direction ranging from N45°W to N20°W on the eastern and northeastern flank. On the northwestern flank, it plunges to a direction from N40°W to N10°W.

The second group of lineation is dominant and penetrative in all of the three tectono-lithologic units of the dome and it represents the dominant deformation. In the upper unit, the lineation is defined by the alignment of metamorphic minerals and stretched quartz; it is also represented by crenulations. In the middle unit, it is formed by alignment of mica grains, stretched quartz ribbons, tails of asymmetric feldspar porphyroclasts and garnet pressure shadows. In the lower unit, the lineation in the paragenesis is defined by alignment of mica, stretched quartz ribbons and elongated feldspar grains, and this deformation also formed the typical banded structure in gneiss. Preferred orientation of hornblendes defines the lineation in the amphibolites. In the margin of core granite pluton, the lineation developed much better than foliation which resulted in the formation of typical L-tectonite.

The second group of lineation has a consistent nearly east–west plunging. It plunges to a direction ranging from S85°W to N85°W on the northwestern flank; it plunges to a direction ranging from N80°E to S80°E on the eastern and northeastern flank.

The third group of lineation is striations plunging to the outsides of the dome, which developed only on the surfaces of the closely-spaced cleavages in the upper unit. It is expressed as thermal striations and mineral fibers. It plunges down the dip of the cleavages outward from the core.

The first and second group of lineation exist both in upper and middle units (Fig. 3f), but the second group overprinted the first group obviously. From upper to lower section in the middle unit (toward the core of the dome with stronger deformation), the second group gradually becomes the absolutely predominant lineation in the dome, whereas the first group becomes the remnant lineation. Moreover, only the second group of lineation can be observed in the gneiss and granite pluton of the lower unit. As for the third groups of lineation, it can be seen only in the cleavages in the upper unit. These indicate a developing sequence for the three groups of lineation: the early north–south plunging lineation was overprinted by the later east–west plunging lineation which represents the dominant deformation. The third group of lineation may indicate a collapse of the Ramba gneiss dome in the later stage.

4.2. Kinematics

Based on the observation and analyses of structure, lithology and lineation, we think that the Ramba gneiss

dome underwent three episodes of deformation represented by the three group of lineation, respectively.

The first episode of deformation is a top-down-to-north-northwest sliding represented by the first group of north–south plunging stretched lineation. Kinematic indicators include S–C fabric in XZ plane and north-northwest-convergent tight folds on the northwestern flank of the Ramba gneiss dome.

The second episode is the dominant deformation represented by the second group of east–west plunging lineation. In the upper and middle units on the northwestern flank of the dome, kinematic indicators along the eastward plunging lineation include S–C foliation (Fig. 3g), asymmetric structures in metamorphic minerals, A-type folds, Z-shape folds, offset and asymmetric puddings of quartz veins, garnet pressure shadows and its rotational structures, domino structure of mica, asymmetric feldspar porphyroclasts. S–C foliation and asymmetric feldspar porphyroclasts also can be seen in the mylonitic gneiss of the lower unit. Slaty cleavage and foliation on the northwestern flank have a dip ranging from northwest to north-northwest; all the indicators show a top-to-east kinematics. This presents an east-directed thrusting on the northwestern side of the Ramba gneiss dome. On the northern flank (south to Gongmuzhi, Fig. 2a), foliation in the middle unit dips northwards. Big grains of feldspar in the mylonitic granite in this unit formed σ-type porphyroclast systems, in which the elongated feldspar grains define the S-foliation, whereas in porphyroclasts' tails, the preferred oriented mica and quartz ribbons form the C-foliation. The relationship between the S and C foliation indicates a top-to-east movement. On the northeastern flank of the dome, the same kinematic indicators along the eastward plunging lineation also indicate a top-to-east sliding, and huge asymmetric puddings are one kind of such indicators (Fig. 3h). Foliation on this flank dips eastwards, thus the kinematics represents an eastward sliding of a normal fault. Top-to-east kinematic indicators can be also found in the margin of the granite pluton, but the deformation becomes weaker toward the core of pluton. Andalusite grains generated by the thermal metamorphism in the country rocks cut the foliation in the middle and lower units, but they also have a preferred orientation (Fig. 3e). This shows that the pluton possibly intruded in a late stage of this deformation episode. The above kinematic analyses show a unified top-down-to-east shear in all the units in the Ramba gneiss dome during the second episode of deformation.

The third episode of deformation is a top-down-to-outside of the Ramba gneiss dome along the hot striations which developed sparsely in the upper unit and the upper detachment fault. This deformation was caused by the collapse of the dome in the latest stage.

5. Thermochronology of leucogranite in the core

Leucogranite exposed in the cores of the domes is one of the most remarkable features in NHGD. The leucogranite pluton in the core of the Ramba gneiss dome has the same deformation and kinematics as those produced by the dominant deformation (the second episode). The deformation becomes weaker toward the center of the pluton; andalusite grains generated by the thermal metamorphism in the country rocks cut the foliation, but they also have a preferred orientation. This shows that the leucogranite intruded in a late stage of the dominant deformation episode, and its cooling ages may give an upper limitation for the age of the dominant deformation. We collected two samples of the fresh leucogranite (see Fig. 2a for the locations) to do the dating with $^{40}Ar/^{39}Ar$ method. The rocks are garnet two-mica granite. Sample T02Q-69 is from the margin of the pluton and biotite was separated for the dating; Sample T02Q-70-1 is from the center of the pluton and muscovite was dated. $^{40}Ar/^{39}Ar$ thermochronological analyses were performed in UCLA. The results are listed in Table 1.

$^{40}Ar/^{39}Ar$ step heating analytical data for the samples are listed in Table 2. The corresponding spectra and inverse isochrones are shown in Fig. 5. All samples have ideal age spectra, indicating that the leucogranite was generated by one thermal event.

Data in Table 1 show that the cooling ages of the leucogranite in the core of the Ramba gneiss dome are about 6 Myr. This indicates that the dominant deformation in the dome has been in its late stage when the pluton cooled down. The Yadong-Gulu rift, to which the Ramba gneiss dome belongs tectonically, probably began to be active since 11 Myr [43] and reached its peak activation at about 8 Myr [44]. Therefore, the activity of Yadong-Gulu rift coincides with the dominant deformation of the Ramba gneiss dome both in tectonic contact and deformation ages. It is reasonable to attribute the dominant deformation (top-down-to-east sliding) in Ramba gneiss dome to the east–west extension of the north–south trending rifts, which widely developed in the northern Himalaya. The emplacement of the leucogranite pluton in a late stage during the dominant deformation formed the doming shape of the dome.

Table 1
Results of $^{40}Ar/^{39}Ar$ analyses on the leucogranite in the core of the Ramba gneiss dome

Sample number	Location	Petrology	Measured mineral	WMPA ±1σ(Myr)	Inverse isochron age		
					Age ±1σ(Ma)	MSWD	Trapped $^{40}Ar/^{36}Ar$
T02Q-69	Margin	Leucogranite	Biotite	6.04 ± 0.13	5.99 ± 0.14	1.562021	300.1664 ± 5.907128
T02Q-70-1	Core	Leucogranite	Muscovite	6.19 ± 0.11	6.15 ± 0.12	0.3029752	297.7110 ± 2.609215

Table 2
$^{40}Ar/^{39}Ar$ step heating analytical data on biotite and muscovite from the leucogranite in the core of Ramba gneiss dome[a]

T (°C)	$(^{40}Ar/^{39}Ar)_m$	$(^{36}Ar/^{39}Ar)_m$	$(^{37}Ar/^{39}Ar)_m$	$(^{38}Ar/^{39}Ar)_m$	^{39}Ar/mol	$(^{40}Ar^*/^{39}ArK)_m \pm 1\sigma$	WMPA $\pm 1\sigma$(Myr)
T02Q-69 biotite W = 6.8 mg J = 0.003571783							
500	36.6872	0.117444	0.28181	0.0657	3.09E-15	1.9733 ± 0.775	12.67 ± 4.96
600	6.5172	0.018993	0.12353	0.0299	1.65E-14	0.8821 ± 0.121	5.67 ± 0.78
700	1.7530	0.002674	0.01766	0.0280	7.50E-14	0.9314 ± 0.029	5.99 ± 0.18
770	1.2598	0.001040	0.02043	0.0275	5.82E-14	0.9214 ± 0.025	5.93 ± 0.16
840	1.4815	0.001798	0.06312	0.0270	1.99E-14	0.9227 ± 0.064	5.94 ± 0.41
900	1.7409	0.002556	0.06872	0.0278	2.04E-14	0.9586 ± 0.071	6.17 ± 0.45
960	1.2791	0.001135	0.03164	0.0280	5.59E-14	0.9136 ± 0.024	5.88 ± 0.15
1050	1.3011	0.001083	0.04826	0.0274	6.21E-14	0.9523 ± 0.021	6.13 ± 0.14
1150	1.7550	0.002245	0.28435	0.0266	2.55E-14	1.0822 ± 0.052	6.96 ± 0.33
T02Q-70-1 muscovite W = 6.9 mg J = 0.003568018							
500	137.4573	0.458471	0.04489	0.1599	1.87E-15	1.9500 ± 2.156	12.51 ± 13.78
600	16.2275	0.051085	0.04155	0.0289	2.94E-15	1.1026 ± 0.634	7.08 ± 4.06
700	5.1078	0.013699	0.01124	0.0155	9.18E-15	1.0280 ± 0.154	6.61 ± 0.99
770	4.2801	0.010995	0.00378	0.0149	1.75E-14	0.9985 ± 0.099	6.42 ± 0.63
840	6.4428	0.018351	0.00102	0.0160	6.23E-14	0.9875 ± 0.058	6.35 ± 0.38
880	1.5977	0.002038	0.00028	0.0128	1.60E-13	0.9626 ± 0.013	6.19 ± 0.08
920	1.7637	0.002694	0.00055	0.0129	6.50E-14	0.9347 ± 0.028	6.01 ± 0.18
960	2.2327	0.004170	0.00087	0.0131	3.66E-14	0.9675 ± 0.054	6.22 ± 0.35
1000	2.1571	0.004081	0.00041	0.0132	3.39E-14	0.9184 ± 0.045	5.90 ± 0.29
1070	1.8293	0.002784	0.00017	0.0129	8.46E-14	0.9738 ± 0.020	6.26 ± 0.13
1150	1.5220	0.001766	0.00023	0.0127	1.07E-13	0.9673 ± 0.018	6.22 ± 0.12
1350	3.6520	0.008785	0.00014	0.0143	2.67E-14	1.0232 ± 0.074	6.57 ± 0.47

[a] *m* represents isotope ratio measured by mass-spectrometer. $^{40}Ar/^{39}Ar$ analyses were performed in UCLA, and detailed analytical procedures can be found in Ref. [45]. Separated minerals and flux monitors were irradiated in Ford reactor, University of Michigan, for 45 h. Reactor neutron flux was determined using sanidine standard Fish Canyon Tuff (27.8 Myr) [46]. After irradiation, samples were step heated in a Ta crucible in a double vacuum furnace and isotopic compositions of the released gas were determined using a gas-source automated mass-spectrometer. Plateau and isochron ages were calculated with a program, AGECAL.EXE. Age uncertainties are reported at the 1σ level, and they do not include the uncertainties in J-Factors or decay constants.

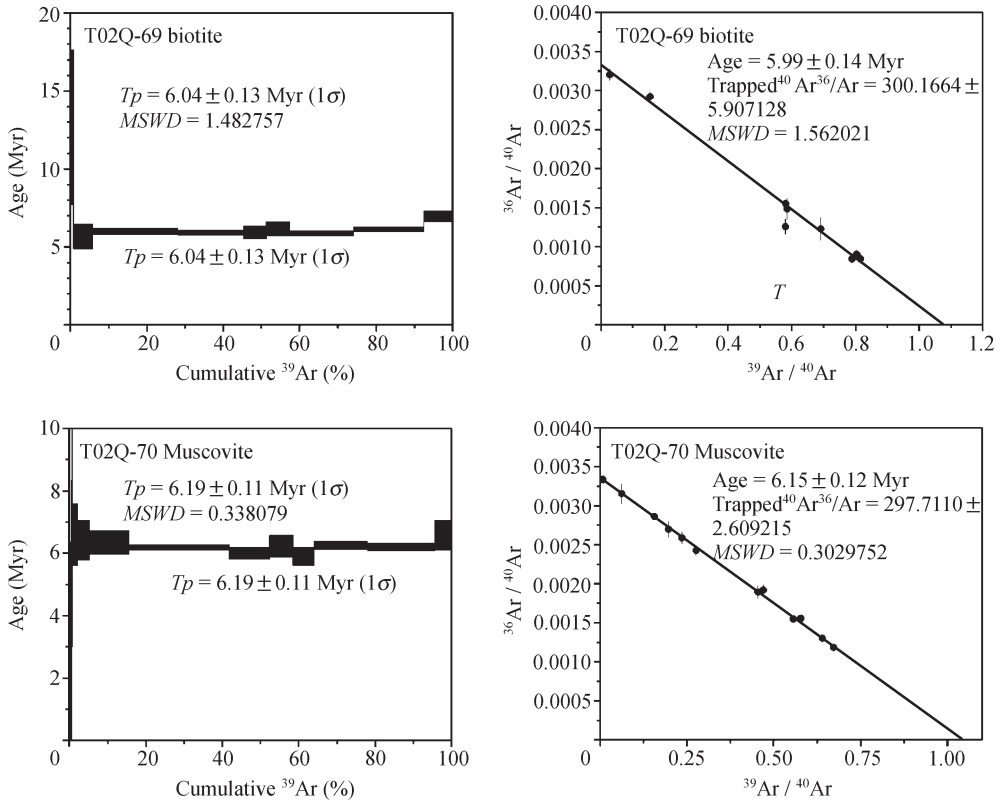

Fig. 5. $^{40}Ar/^{39}Ar$ age spectra and inverse isochrones for the leucogranite in the core of the Ramba gneiss dome.

6. Discussion on the formation mechanism of the Ramba gneiss dome

Many different formation mechanisms have been put forward for the gneiss domes in NHGD, such as diapirism, thrust ramp, channel flow and detachment-metamorphic core complex [1,3,4,6,9,16,23,28–34]. But unfortunately, any single formation mechanism cannot be used to explain well the three episodes of deformation in the Ramba gneiss dome.

The early top-down-to-north-northwest sliding is preserved in the upper and middle unit of the Ramba gneiss dome except the lower unit and granite pluton. This may be the deformation preserved in the Tethyan Himalayan sequence formed by the northward detachment along the STDS. Some recent studies also reported similar kinematics in other gneiss domes of NHGD [6,7,24].

The dominant deformation in Ramba gneiss dome is a unique top-down-to-east shear. It is quite different from the deformation in Kangmar, Yalashangbo, Malashan and Kampa domes, in which the major deformation is in a north–south trend (related to the north–south extension of the STDS). Therefore, we suggest that the formation mechanism of the Ramba gneiss dome is similar to that of Leo Pargil dome and Gurla Mandhata dome in western NHGD [26,27], these two domes were formed by the east–west extension along the north–south trending rifts in Tibet. Reasons for this conclusion are listed below.

Firstly, the Ramba gneiss dome is composed of high-grade metamorphic rocks intruded by younger pluton and structurally overlain by low-grade rocks. The slate and meta-sandstone of the sedimentary sequence above the upper detachment fault made up the hanging wall, while the mylonitic paragneiss, amphibolites and leucogranite beneath the lower detachment fault composed the footwall. The contact between two walls is an intensively deformed ductile shear zone, i.e., the middle unit confined by the upper and lower detachment faults. Mylonitic schist constituted this unit which may be the basal part of the upper unit experiencind detachment shear [24]. Therefore, the lower detachment fault may be the basal or main detachment fault in Ramba gneiss dome that separates the hanging wall composed of sedimentary sequence from the footwall of crystalline basement. The dominant deformation in this detachment fault is a top-down-to-east shear related to an east–west extension. This indicates a formation mechanism for Ramba gneiss dome similar to that of detachment-metamorphic core complex. Ductile deformation in the middle, lower unit and the lower detachment fault is the result of east–west extension.

Secondly, the present shape of Ramba gneiss dome may result from the emplacement of the leucogranite pluton in a late stage of the dominant deformation. Besides the diapir of the pluton, tectonic thinning and isostatic rebounding also contributed to doming of the area which caused the third episode of deformation – the collapse sliding toward the outsides of the dome.

Thirdly, the Ramba gneiss dome is located in the Yadong-Gulu rift. Its eastern flank is truncated by a north–south trending normal fault which may be a part of the Yadong-Gulu rift (Fig. 2). $^{40}Ar/^{39}Ar$ thermochronology of leucogranite with cooling ages of about 6 Ma emplaced in the late stage of the dominant deformation also indicates that the age of dominant deformation in Ramba gneiss dome is simultaneous with the north–south trending rifts widely developed in northern Himalaya.

Therefore, we believe that the Ramba gneiss dome underwent an early top-down-to-north-northwest sliding (possibly related to the activity of the STDS), then a top-down-to-east dominant shear deformation (possibly related to the east–west extension of the north–south trending rifts), and finally the emplacement of the leucogranite pluton in the late stage of the dominant deformation episode which caused the collapse sliding toward the outsides of the dome. The formation of the tectonic units in Ramba gneiss dome is possibly a result of the east–west extension.

7. Conclusion

The Ramba gneiss dome is located in the northern part of the NHGD. It is made up by mylonitic gneisses and granite pluton, and overlain structurally by low-grade metamorphic rocks. This dome consists of three tectonolithologic units separated by two detachment faults (the upper and lower detachment fault). The lower detachment fault is the basal or main detachment fault that separates the hanging wall composed of Tethyan Himalayan sedimentary sequence from the footwall composed of mylonitic gneisses. The middle unit between the upper and the lower detachment fault is the basal part of the upper unit intensively deformed by ductile deformation. The Ramba gneiss dome underwent three episodes of deformation corresponding to the three groups of lineation, respectively. The first episode of deformation is a top-down-to-north-northwest sliding possibly related to the activity of the STDS. The second episode is the dominant deformation with a unique top-down-to-east kinematics, which resulted in the major tectonic features of the dome. The third episode of deformation is a collapse sliding toward the outsides of the dome. The leucogranite pluton in the core of the dome emplaced in a late stage of the dominant deformation with $^{40}Ar/^{39}Ar$ cooling ages of about 6 Ma. Integrating tectonic features and thermochronology, we think that the formation of the Ramba gneiss dome is possibly related to the activity of the north–south trending rifts in Tibetan plateau and may be the result of the east–west extension and magmatic diapir.

Acknowledgement

This work was supported by National Natural Science Foundation of China (Grant No. 40572115).

References

[1] Burg JP, Guiraud M, Chen GM, et al. Himalayan metamorphism and deformation in the North Himalayan belt, southern Tibet, China. Earth Planet Sci Letts 1984;69:391–400.

[2] Chen Z, Liu Y, Hodges KV, et al. Structural evolution of the Kangmar dome: a metamorphic core complex in southern Xizang (Tibet). Science 1990;250:1552–6.

[3] Wu C, Nelson KD, Wortman G, et al. Yadong cross structure and South Tibetan detachment in the east central Himalaya (89–90°E). Tectonics 1998;17:28–45.

[4] Hauck ML, Nelson KD, Brown LD, et al. Crustal structure of the Himalayan orogen at approximately 90 east longitude from Project INDEPTH deep reflection profile. Tectonics 1998;17:481–500.

[5] Lee J, Hacker BR, Dinklage WS, et al. Evolution of the Kangmar dome, southern Tibet: Structural, petrologic, and thermochronologic constraints. Tectonics 2000;19:872–95.

[6] Lee J, Wang Y, McWilliams M, et al. Contraction, extension, and diapirism in Mabja Dome: implications for tectonics of southern Tibet. Geol Soc Am Abstr 2002;34:332.

[7] Lee J, Hacker B, Wang Y. Evolution of north Himalayan gneiss domes: structural and metamorphic studies in Mabja Dome, southern Tibet. J Struct Geol 2004;26:2297–316.

[8] Burg JP, Brunel M, Gapais D, et al. Deformation of the crystalline main central sheet in south Tibet (China). J Struct Geol 1984;6:535–42.

[9] Burg JP, Chen JM. Tectonics and structural zonation of southern Tibet, China. Nature 1984;311:219–23.

[10] Burchfiel BC, Chen Z, Hodges KV, et al. The south Tibetan detachment system, Himalayan orogen, extension contemporaneous with and parallel to shortening in a collisional mountain belt. Geol Soc Am Special Paper 1992;269:1–41.

[11] Hodges KV, Parrish R, Housh T, et al. Simultaneous Miocene extension and shortening in the Himalayan orogen. Science 1992;258:1466–70.

[12] Coleman M, Hodges K. Evidence for Tibetan plateau uplift before 14 Myr age from a new minimum age for east–west extension. Nature 1995;374:49–52.

[13] Harrison TM, Copeland P, Kidd WSF, et al. Activation of the Nyainqentanghla shear zone: implication uplift of the southern Tibetan plateau. Tectonics 1995;14:658–76.

[14] Searle MP. The rise and fall of Tibet. Nature 1995;347:17–8.

[15] Seeber L, Pêcher A. Strain partitioning along the Himalayan arc and the Nanga Parbat antiform. Geology 1998;26:791–4.

[16] Yin A, Kapp PA, Murphy MA, et al. Significant late Neogene east–west extension in northern Tibet. Geology 1999;27:787–90.

[17] Yin A. Mode of Cenozoic east–west extension in Tibet suggesting a common origin of rifts in Asia during the Indo-Asian collision. J Geophys Res 2000;105(B9):21745–59.

[18] Zhang JJ, Guo L. Structure and geochronology of the southern Xainza-Dinggye rift and its relationship to the south Tibetan detachment system. J Asian Earth Sci 2007;29:722–36.

[19] Zhang JJ, Ding L, Zhong DL, et al. Orogen-paraller extension in Himalaya. Is it the indicator of collapse or the product of compressive uplift? Chinese Sci Bull 2000;45:114–9.

[20] Zhang JJ, Guo L, Ding L. Structural characteristics of middle and southern Xainza-Dinggye normal fault system and its relationship to southern Tibetan detachment system. Chinese Sci Bull 2002;47:1063–9, [in Chinese].

[21] Zhang JJ, Ding L. East–west extension in Tibetan plateau and its significance to tectonic evolution. Chinese J Geol 2003;38:179–89, [in Chinese].

[22] Yin A, Harrison TM. Geologic evolution of the Himalayan–Tibetan orogen. Annu Rev Earth Planet Sci 2000;28:211–80.

[23] Li DW, Liu DM, Liao QA, et al. Definition and significance of the Lhagoi Kangri metamorphic core complexes in Sa'gya, southern Tibet. Reg Geol China 2003;22:7–11, [in Chinese].

[24] Zhang JJ, Guo L, Zhang B. Structure and kinematics of the Yalashangbo dome in the northern Himalayan dome belt, China. Chinese J Geol 2007;42(1):16–30, [in Chinese].

[25] Zhang JY, Liao QA, Li DW, et al. Laguigangri Leucogranites and its relation with Laguigangri metamorphic core complex in Sajia, south Tibet. Earth Sci—J China Univ Geosci 2003;28:695–701, [in Chinese].

[26] Thiede RC, Ramon Arrowsmith J, Bookhagen B, et al. Dome formation and extension in the Tethyan Himalaya, Leo Pargil, northwest India. Geol Soc Am Bull 2006;118(5–6):635–50.

[27] Murphy AM, Yin A, Kapp P, et al. Structural evolution of the Gurla Mandhata detachment system, southwest Tibet: implications for the eastward extent of the Karakoram fault system. Geol Soc Am Bull 2002;114:428–47.

[28] Harrison TM, Lovera OM, Grove M. New insights into the origin of two contrasting Himalayan granite belts. Geology 1997;25:899–902.

[29] Le Fort P. Metamorphism and magmatism during the Himalayan collision. Geological Society of London Special Publication; 1986. p. 159–72.

[30] Le Fort P, Cuney M, Deniel C, et al. Crustal generation of Himalayan leucogranites. Tectonophysics 1987;134:39–57.

[31] Beaumont C, Jamieson RA, Nguyen MH, et al. Himalayan tectonics explained by extrusion of a low-viscosity crustal channel coupled to focused surface denudation. Nature 2001;414:738–42.

[32] Beaumont C, Jamieson RA, Nguyen MH, et al. Crustal channel flows: numerical models with applications to the tectonics of the Himalayan–Tibetan orogen. J Geophys Res 2004;109(B6):B06406.

[33] Makovsky Y, Klemperer SL, Ratschbacher L, et al. Midcrustal reflector on INDEPTH wide-angle profiles: an ophiolite slab beneath the India–Asia suture in southern Tibet? Tectonics 1999;18:793–808.

[34] Yin A. Cenozoic tectonic evolution of the Himalayan orogen as constrained by along-strike variation of structural geometry, exhumation history, and foreland sedimentation. Earth Sci Rev 2006;76:1–131.

[35] Hodges KV. Tectonics of the Himalaya and southern Tibet from two perspectives. Geol Soc Am Bull 2000;112:324–50.

[36] Gansser A. The geology of the Himalayas. New York: Wiley Interscience; 1964, p. 1–289.

[37] Le Fort P. Himalayas: the collision range. Present knowledge of the continental arc. Am J Sci 1975;275:1–44.

[38] Searle MP. Stratigraphy, structure and evolution of the Tibetan–Tethys zone in Zanskar and the Indus suture zone in the Ladakh Himalaya. Trans R Soc Edinburgh Earth Sci 1983;73:205–19.

[39] Ratschbacher L, Frisch W, Liu G, et al. Distributed deformation in southern and western Tibet during and after the India–Asia collision. J Geophys Res 1994;99:19917–45.

[40] Quidelleur X, Grove M, Lovera OM, et al. The thermal evolution and slip history of the Renbu Zedong Thrust, southeastern Tibet. J Geophys Res 1997;102:2659–79.

[41] Yin A, Harrison TM, Ryerson FJ, et al. Tertiary structural evolution of the Gandese thrust system, southeastern Tibet. J Geophys Res 1994;99:18175–201.

[42] Chengdu Institute of Geology and Mineral Resources, China Geological Survey. Geological maps of the Qinghai-Tibet plateau and its adjacent regions (1:1000 000). Chengdu Cartographic Publishing House, China, 2004 [in Chinese].

[43] Pan Y, Kidd WSF. Nyainqentanghla shear zone: A late Miocene extensional detachment in the southern Tibetan. Geology 1993;20:775–8.

[44] Harrison TM, Mckeegan KD, Le Fort P. Detection of inherited Monazite in the Manaslu leucogranite by 208 Pb/232 Th ion microprobe dating, crystallization age and tectonic implication. Earth Planet Sci Letts 1995;133:271–82.

[45] McDougall I, Harrison TM. Geochronology and thermochronology by the 40Ar/39Ar method. 2nd ed. New York: Oxford University Press; 1999.

[46] Cebula GT, Kunk MJ, Mehnert HH, et al. The Fish Canyon Tuff, a potential standard for the 40–39 Ar and fission-track dating methods. Terra Cognita 1986;6:139–40.